Supplemental Information

Figure S1. Characterization of Lentiviral Spread and Estimation of *in vivo* Lentivirus Multiplicity of Infection, Related to Figure 1.

Figure S2. Coverage and Performance of shRNA and sgRNA Pooled Libraries *in vivo*, Related to Figure 1.

Figure S3. Comparison of Striatal-Enriched Genes and Core Essential Genes (CEG2) to Candidate Neuronal Essential Genes Identified in shRNA and CRISPR Screens, Related to Figures 2 and 3.

Figure S4. Identification of Candidate Protective and Vulnerability Factors in HD Mouse Models, Related to Figure 4.

Figure S5. Levels of *Nme1* Expression in Mouse and Human Brain, and Effects of *Nme1* knockdown and overexpression *in vivo* and *in vitro*, Related to Figure 5.

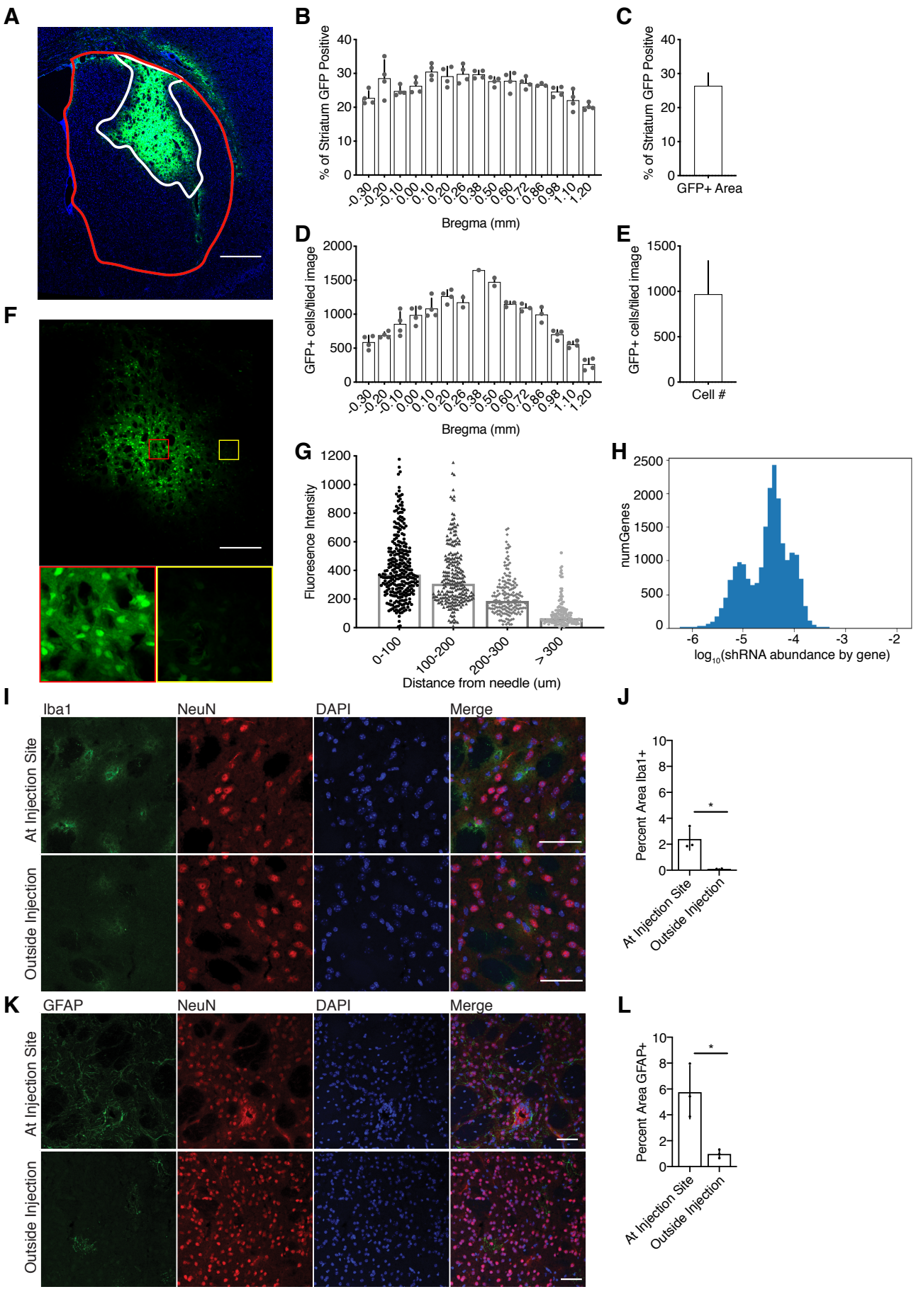
A
B
% of Striatum GFP Positive
Bregma (mm)
C
% of Striatum GFP Positive
GFP+ Area
D
GFP+ cells/tiled image
Bregma (mm)
E
GFP+ cells/tiled image
Cell #
F
G
Fluoresence Intensity
0-100
100-200
200-300
>300
Distance from needle (um)
H
numGenes
log10(shRNA abundance by gene)
I
Iba1
NeuN
DAPI
Merge
At Injection Site
Outside Injection
J
Percent Area Iba1+
At Injection Site
Outside Injection
K
GFAP
NeuN
DAPI
Merge
At Injection Site
Outside Injection
L
Percent Area GFAP+
At Injection Site
Outside Injection

Figure S1. Characterization of Lentiviral Spread and Estimation of *in vivo* Lentivirus Multiplicity of Infection, Related to Figure 1. **(A)** Representative image of control, GFP cDNA lentiviral spread after injection into the adult striatum. Scale bar = 400μm. **(B)** Area of the striatum (red line in panel A) positive for GFP viral infection (white line in panel A) was measured for each section from anterior to posterior across the injection sites. The percent GFP-positive area present in 4 serial coronal sections is represented as mean and standard deviation (SD) for each coordinate relative to Bregma (mm). **(C)** The GFP positive area (effective viral coverage) across the injection sites is 26.41% of the striatum, $n = 60$ sections. **(D)** GFP positive cells were manually counted in maximum intensity projections of serial 20x 10μm Z-stacks of the GFP positive injection area. The number of GFP positive cells for 4 serial sections is represented as mean + SD for each coordinate relative to Bregma (mm). **(E)** Bar graph of the average number of GFP-positive cells per 10μm Z-stack of a 20μm section, $n = 56$ sections. Together the viral spread and number of cells counted per 10μm section indicate ~120,000 neurons are infected per striatal hemisphere (see STAR Methods for details). Bars represent mean + SD. **(F)** Representative image of endogenous fluorescence intensity of GFP-positive cells in a tissue section directly adjacent to the injection site (red box) vs. at the periphery of the injection (yellow box). Scale bar = 50μm. **(G)** Endogenous fluorescence intensity of individual cells was measured from summed intensity projections of tiled 20μm Z-stacks to evaluate *in vivo* MOI. Median fluorescence intensity in arbitrary units at the periphery is 65.32, while at the needle track is 371.00, indicating a 5.68-fold range in the distribution of viral integration events. $n > 165$ cells per distance bin from 4 coronal sections, bars represent median value. **(H)** Histogram of the distribution of $\log_{10}$ shRNA read counts by gene in the input library shows the relative abundance of the total shRNA targeting each gene. **(I)** Iba1, and **(K)** GFAP co-stained with NeuN and DAPI in virus-injected striatum of C57Bl/6J control mice. 40x z-stack images were taken at the center of the injection site and compared to a region peripheral to the injection site. **(J/L)** Quantification of Iba1 and GFAP staining showed a small localized increase in inflammatory markers adjacent to the center of the injection site, but not peripheral to the injection, $n = 3$, * p-value < 0.05; two-tailed student's *t*-test. Images have been modified to increase contrast for visualization purposes. All images were modified identically and quantification was performed on unmodified images as described in the methods.

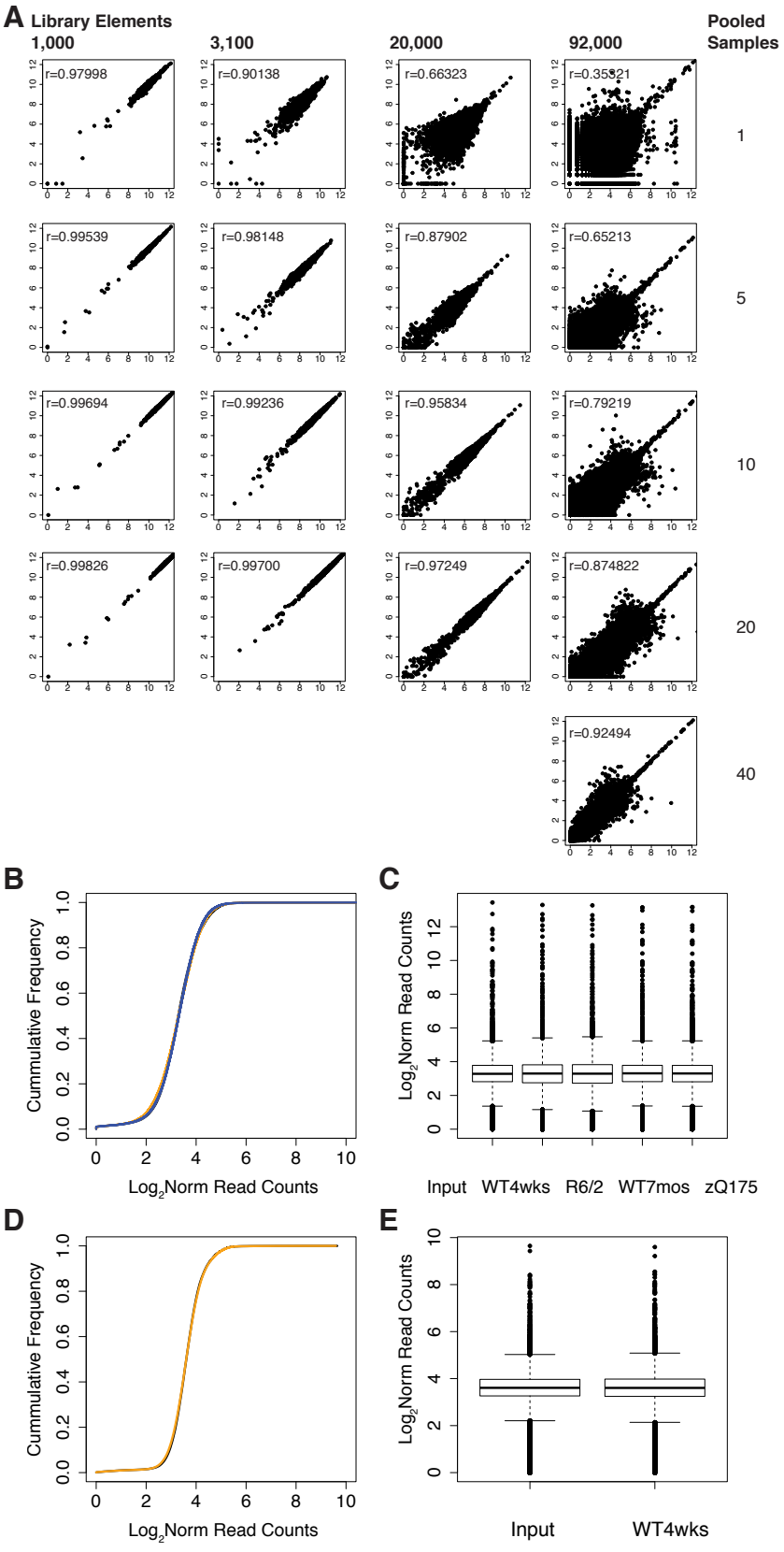
A
Library Elements
1,000
3,100
20,000
92,000
Pooled Samples
r=0.97998
r=0.90138
r=0.66323
r=0.35821
1
r=0.99539
r=0.98148
r=0.87902
r=0.65213
5
r=0.99694
r=0.99236
r=0.95834
r=0.79219
10
r=0.99826
r=0.99700
r=0.97249
r=0.874822
20
r=0.92494
40
B
Cummulative Frequency
Log2Norm Read Counts
C
Log2Norm Read Counts
Input
WT4wks
R6/2
WT7mos
zQ175
D
Cummulative Frequency
Log2Norm Read Counts
E
Log2Norm Read Counts
Input
WT4wks

Figure S2. Coverage and Performance of shRNA and sgRNA Pooled Libraries *in vivo*, Related to Figure 1. **(A)** Representative scatterplots of the $\log_2$ normalized read counts in libraries of low to high complexity (1,000; 3,100; 20,000; and 92,000 elements). Pooling higher numbers of samples (1, 5, 10, 20, and 37) into a single replicate reduces variation and increases the Pearson correlation coefficient (r) as shown for each comparison. A single replicate is sufficient for full coverage and high correlation ($r > 0.75$) of small 1,000 and 3,100 element libraries, while pooling of many samples per replicate is required for the 20,000 and 92,000 element libraries. **(B)** Cumulative density function (CDF) plot of the cumulative frequency vs. the $\log_2$ normalized representation of shRNAs in the genome-wide library. The WT control replicates both 4 weeks (blue) and 7 months (orange) of *in vivo* incubation are similar to the plasmid input (black). **(C)** Boxplot of the distributions of $\log_2$ normalized read counts in the shRNA screening data sets as compared to the plasmid input. **(D)** CDF plot of the cumulative frequency vs. the $\log_2$ normalized representation of sgRNAs in the input library (black) and the WT 4 weeks samples (orange). **(E)** Boxplot of the distributions of $\log_2$ normalized read counts in the sgRNA screening data sets as compared to the plasmid input. Together these plots illustrate recovery of the library at a depth sufficient for analysis of differential library representation in the pooled replicate samples.

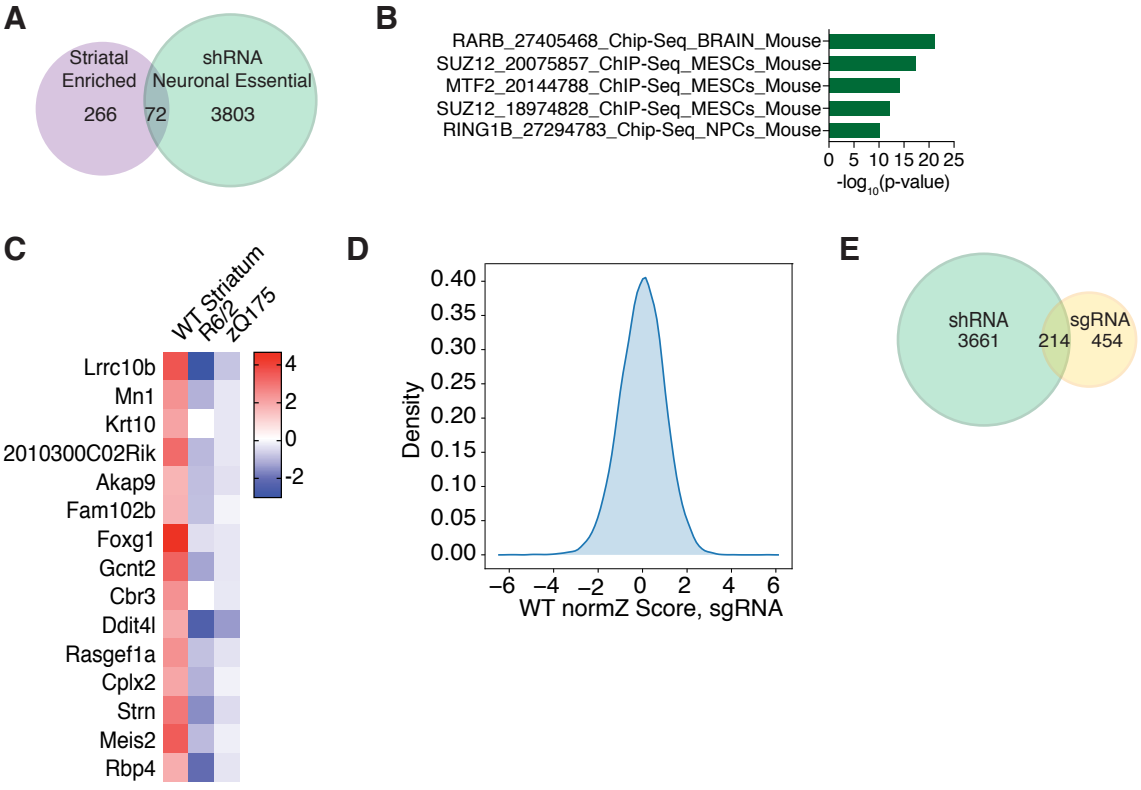
A
Striatal Enriched
266
72
shRNA Neuronal Essential
3803
B
RARB_27405468_Chip-Seq_BRAIN_Mouse
SUZ12_20075857_ChIP-Seq_MESCs_Mouse
MTF2_20144788_ChIP-Seq_MESCs_Mouse
SUZ12_18974828_ChIP-Seq_MESCs_Mouse
RING1B_27294783_Chip-Seq_NPCs_Mouse
0 5 10 15 20 25
-log10(p-value)
C
WT Striatum
R6/2
zQ175
Lrrc10b
Mn1
Krt10
2010300C02Rik
Akap9
Fam102b
Foxg1
Gcnt2
Cbr3
Ddit4l
Rasgef1a
Cplx2
Strn
Meis2
Rbp4
4
2
0
-2
D
Density
0.40
0.35
0.30
0.25
0.20
0.15
0.10
0.05
0.00
−6 −4 −2 0 2 4 6
WT normZ Score, sgRNA
E
shRNA
3661
214
sgRNA
454

Figure S3. Comparison of Striatal-Enriched Genes and Core Essential Genes (CEG2) to Candidate Neuronal Essential Genes Identified in shRNA and CRISPR Screens, Related to Figures 2 and 3. **(A)** Venn diagram of overlap between striatal enriched genes [>1.5 $\log_2$ fold-change enrichment in striatum vs. rest of brain (Kasukawa et al., 2011)] and neuronal essential genes identified in the WT shRNA screen. **(B)** ChEA analysis of the 72 neuronal essential genes which display > 1.5 $\log_2$ fold-change striatal enriched expression (overlap in panel A, and listed in Table S2), to identify putative regulators of these genes from published chromatin immunoprecipitation studies. Results represented as Fisher's exact test $-\log_{10}$ p-value**.** **(C)** Heatmap of the top 15 candidate neuronal essential genes with enriched expression in the striatum vs. the rest of the brain (left column, fold enrichment in striatum). All of these genes have significantly decreased expression (corrected p-value < 0.05) in the striatum of the either the R6/2 or zQ175 HD mouse models, or both (right two columns, fold downregulation in HD model). **(D)** Density plot of normZ scores for the WT CRISPR screen shows normal distribution. **(E)** Venn diagram of the overlap of neuronal essential genes identified by both the shRNA and CRISPR sgRNA screens, hypergeometric p-value = 0.023.

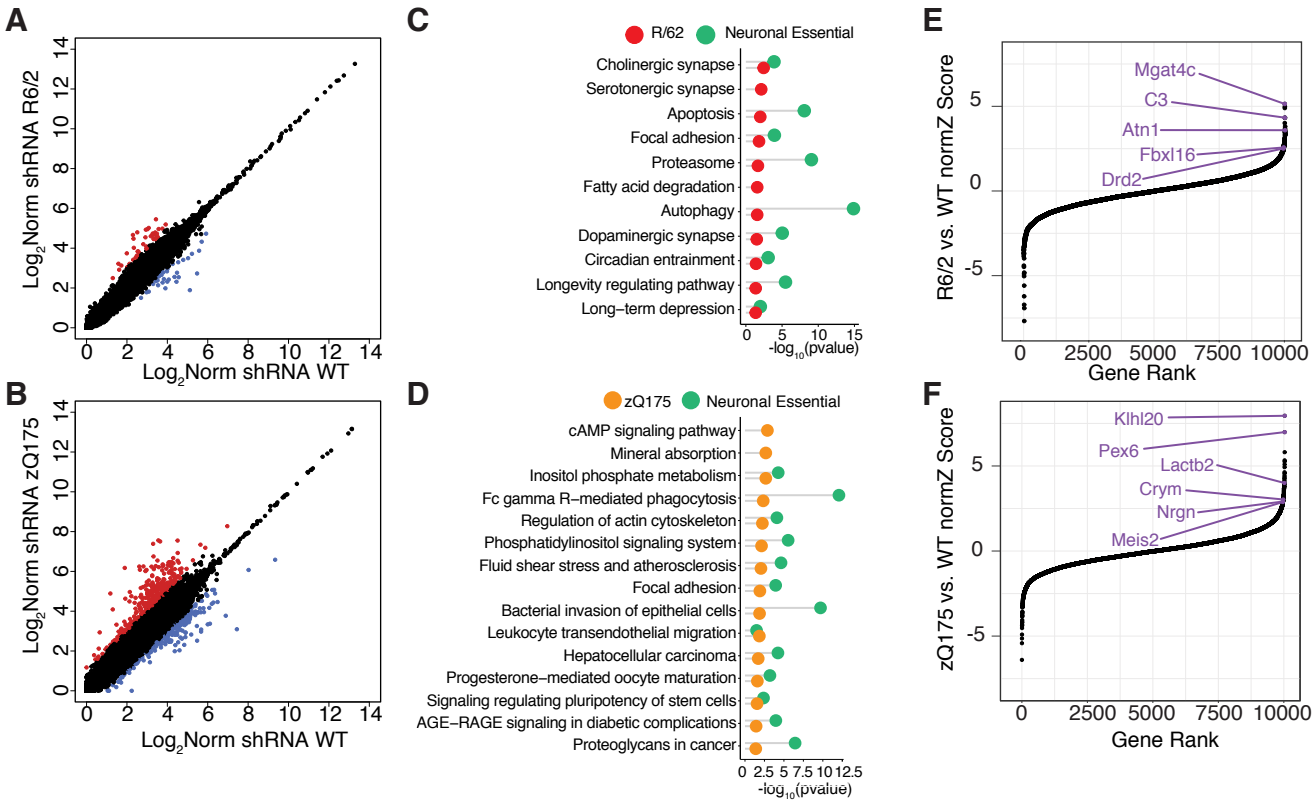
A
Log2Norm shRNA R6/2
Log2Norm shRNA WT
B
Log2Norm shRNA zQ175
Log2Norm shRNA WT
C
R/62
Neuronal Essential
Cholinergic synapse
Serotonergic synapse
Apoptosis
Focal adhesion
Proteasome
Fatty acid degradation
Autophagy
Dopaminergic synapse
Circadian entrainment
Longevity regulating pathway
Long−term depression
-log10(pvalue)
D
zQ175
Neuronal Essential
cAMP signaling pathway
Mineral absorption
Inositol phosphate metabolism
Fc gamma R−mediated phagocytosis
Regulation of actin cytoskeleton
Phosphatidylinositol signaling system
Fluid shear stress and atherosclerosis
Focal adhesion
Bacterial invasion of epithelial cells
Leukocyte transendothelial migration
Hepatocellular carcinoma
Progesterone−mediated oocyte maturation
Signaling regulating pluripotency of stem cells
AGE−RAGE signaling in diabetic complications
Proteoglycans in cancer
-log10(pvalue)
E
R6/2 vs. WT normZ Score
Mgat4c
C3
Atn1
Fbxl16
Drd2
Gene Rank
F
zQ175 vs. WT normZ Score
Klhl20
Pex6
Lactb2
Crym
Nrgn
Meis2
Gene Rank

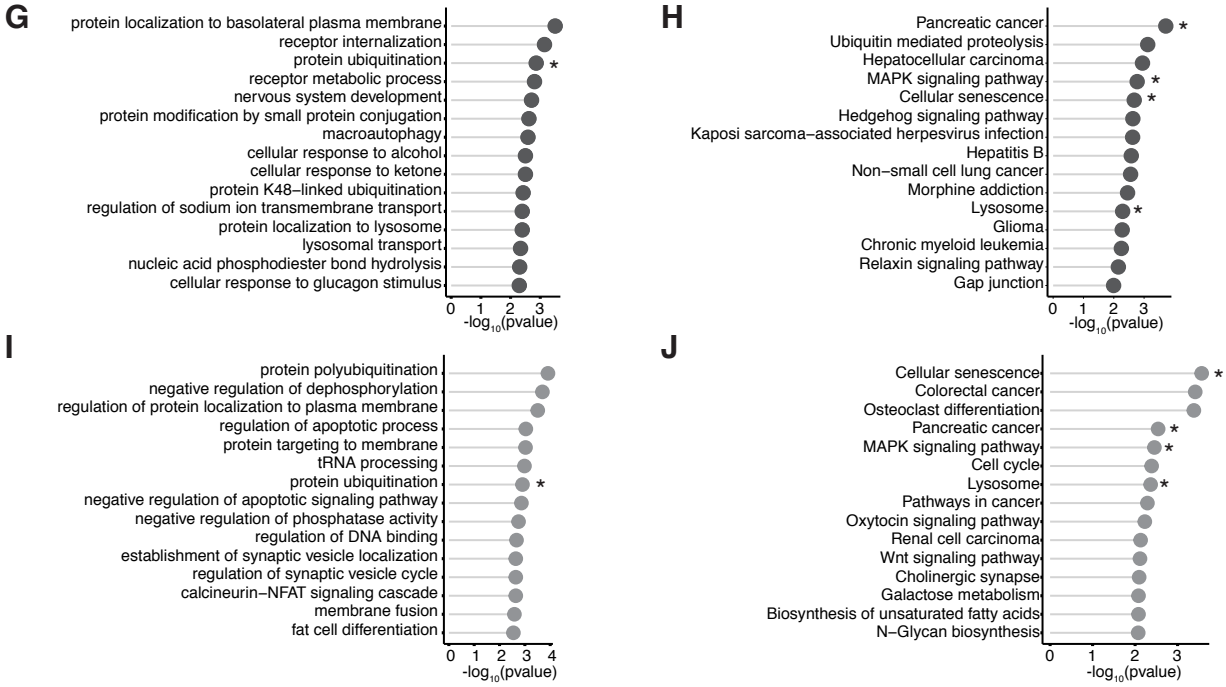
G
protein localization to basolateral plasma membrane
receptor internalization
protein ubiquitination
receptor metabolic process
nervous system development
protein modification by small protein conjugation
macroautophagy
cellular response to alcohol
cellular response to ketone
protein K48−linked ubiquitination
regulation of sodium ion transmembrane transport
protein localization to lysosome
lysosomal transport
nucleic acid phosphodiester bond hydrolysis
cellular response to glucagon stimulus
-log10(pvalue)
H
Pancreatic cancer
Ubiquitin mediated proteolysis
Hepatocellular carcinoma
MAPK signaling pathway
Cellular senescence
Hedgehog signaling pathway
Kaposi sarcoma−associated herpesvirus infection
Hepatitis B
Non−small cell lung cancer
Morphine addiction
Lysosome
Glioma
Chronic myeloid leukemia
Relaxin signaling pathway
Gap junction
-log10(pvalue)
I
protein polyubiquitination
negative regulation of dephosphorylation
regulation of protein localization to plasma membrane
regulation of apoptotic process
protein targeting to membrane
tRNA processing
protein ubiquitination
negative regulation of apoptotic signaling pathway
negative regulation of phosphatase activity
regulation of DNA binding
establishment of synaptic vesicle localization
regulation of synaptic vesicle cycle
calcineurin−NFAT signaling cascade
membrane fusion
fat cell differentiation
-log10(pvalue)
J
Cellular senescence
Colorectal cancer
Osteoclast differentiation
Pancreatic cancer
MAPK signaling pathway
Cell cycle
Lysosome
Pathways in cancer
Oxytocin signaling pathway
Renal cell carcinoma
Wnt signaling pathway
Cholinergic synapse
Galactose metabolism
Biosynthesis of unsaturated fatty acids
N−Glycan biosynthesis
-log10(pvalue)

Figure S4. Identification of Candidate Protective and Vulnerability Factors in HD Mouse Models, Related to Figure 4. (A and B) Scatterplots (corresponding to Figure 4B and 4D) illustrating the correlation of $\log_2$ normalized read counts in the R6/2 and zQ175 screens respectively. Points represent individual shRNA hairpins enriched (red) or depleted (blue) with > 2-fold differential shRNA sequencing representation in the mutant as compared to the isogenic WT control. Highly correlated sequences with a $\log_2$ normalized value greater than 8 are shRNAs that are highly represented in the library, but are not differentially recovered in the screen. **(C and D)** Top KEGG pathways significantly associated with candidate essential genes (knockdown is harmful, library elements are depleted as described in the main text) unique to either the R6/2 (red) and zQ175 (orange) screens respectively, and not identified as essential in the WT neuronal essential shRNA screen, represented with Fisher's exact test $-\log_{10}$ p-value. Even though these genes were not identified as essential in the WT neuronal essential shRNA screen, there was still pathway overlap evident with WT neuronal essential genes (green). **(E and F)** Plot of normZ scores vs. rank of candidate mHTT vulnerability factors (knockdown is protective, library elements in this case are enriched) identified by DrugZ. The top genes from each arm of the screen are labeled in purple. Top **(G and I)** KEGG pathways and **(H and J)** GO terms significantly associated with candidate vulnerability factors in the R6/2 and zQ175 screens respectively, Fisher's exact test expressed as $-\log_{10}$ p-value. Pathways overlapping between the R6/2 and zQ175 screens are marked with an *.

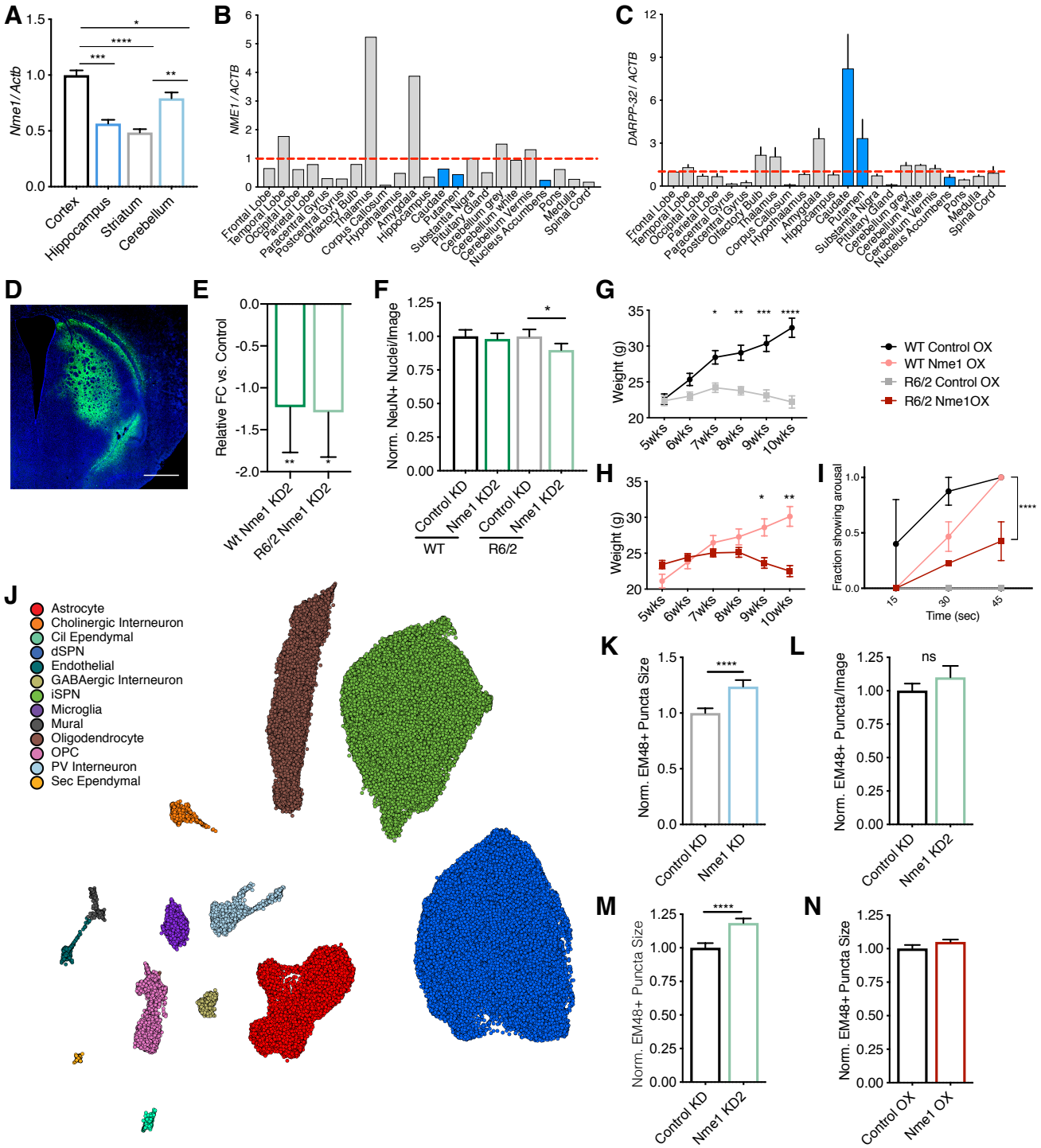
A
Nme1/Actb
Cortex
Hippocampus
Striatum
Cerebellum
B
NME1/ACTB
C
DARPP-32/ACTB
D
E
Relative FC vs. Control
Wt Nme1 KD2
R6/2 Nme1 KD2
F
Norm. NeuN+ Nuclei/Image
Control KD
Nme1 KD2
WT
R6/2
G
Weight (g)
WT Control OX
WT Nme1 OX
R6/2 Control OX
R6/2 Nme1OX
H
I
Fraction showing arousal
Time (sec)
J
Astrocyte
Cholinergic Interneuron
Cil Ependymal
dSPN
Endothelial
GABAergic Interneuron
iSPN
Microglia
Mural
Oligodendrocyte
OPC
PV Interneuron
Sec Ependymal
K
Norm. EM48+ Puncta Size
L
Norm. EM48+ Puncta/Image
M
N
Control OX
Nme1 OX

Figure S5. Levels of *Nme1* expression in mouse and human brain, and effects of *Nme1* knockdown and overexpression *in vivo* and *in vitro,* Related to Figure 5. (A) qRT-PCR of *Nme1* mRNA expression in WT mouse brain regions normalized to *Actb* shows lowest expression of *Nme1* in striatum, $n = 3$ biological replicates. Ordinary one-way ANOVA **** $P < 0.0001$, Tukey's multiple comparison test * $p = 0.027$, ** $p = 0.003$, *** $p = 0.0003$, **** $p < 0.0001$. **(B)** Multiplex Taqman qRT-PCR analysis of a human cDNA array (Origene) confirms low expression of *NME1* (normalized to *ACTB*) in the caudate, putamen, and nucleus accumbens (blue) as compared to overall human brain expression; $n = 1$ array. **(C)** Enriched expression of *DARPP-32* (*PPP1R1B*) in the caudate and putamen (normalized to *ACTB*) in the human cDNA array confirms the specificity of the array panel; $n = 3$ arrays. **(D)** 10x tiled image of a representative GFP AAV9 viral spread area in the striatum upon stereotaxic intracranial injection (Scale bar = 300μm). Contrast in GFP and DAPI images was increased for visualization purposes. **(E)** qPCR quantification of the relative fold-change of *Nme1* mRNA expression in the *Nme1* KD2 as compared to Control KD injected hemispheres to confirm knockdown with a second *Nme1* shRNA hairpin sequence, $n = 10$, ** = p-value = 0.0097, * p-value = 0.013; one-tailed, paired student's *t*-test of DeltaCt values. **(F)** Quantification of NeuN-positive cells in the Control KD vs. *Nme1* KD2 injected striatal hemispheres of WT ($n = 4$) and R6/2 ($n=3$) mice. Points are an average of three images per section from 8 or 16 sections; one-tailed, paired *t*-test, p-value = 0.01. **(G)** Effect of striatal Control OX on the body weights of WT or R6/2 HD model mice. Two-way repeated measures ANOVA p-value genotype <0.0001 with Sidak's, multiple comparison test, * $p = 0.013$, ** $p = 0.0046$, *** $p = 0.0006$, **** $P < 0.00001$. **(H)** Effect of striatal Nme1 OX on body weight of WT vs. R6/2 HD model mice. Two-way repeated measures ANOVA with Sidak's multiple comparison test, ** $p = 0.0013$, and **** $P < 0.0001$. **(I)** Effect of striatal Control OX or striatal *Nme1* OX on the arousability (at 9 weeks of age, 4 weeks after viral transduction) of WT or R6/2 HD model mice. Two-way repeated measures ANOVA p-value genotype = 0.017 with Sidak's, multiple comparison test, **** p-value <0.0001 WT Control OX and WT Nme1 OX vs. R6/2 Control OX. **(J)** ACTIONet graphs of the major annotated cell types in the R6/2 model of HD ($n = 95,885$ nuclei across 20 mice: 5 WT and 5 R6/2 model mice, each for Control and *Nme1* OX). **(K)** Quantification of EM48+ puncta size in Control KD vs. *Nme1* KD injected hemispheres of R6/2 mice ($n = 3$). **(L and M)** Quantification of mHTT aggregates as normalized EM48+ puncta per image and size of EM48+ puncta in Control KD vs. *Nme1* KD2 injected hemispheres of R6/2

mice (n = 3). Panels K-M, points are an average of three images per section from 16 sections, **** p-value < 0.0001; one-tailed paired student's t-test. **(N)** Quantification of EM48+ puncta size in Control OX vs. Nme1 OX injected hemispheres of R6/2 mice (n = 4). Points are an average of three images per section from 8 sections; n.s. one-tailed paired student's t-test. All error bars represent mean and +/- SEM.